Modification of Hemodynamics in Basilar Artery Aneurysm by the Single and Y Stent Placement

Tatsuya Matsuda[a], Yasumasa Ito [a,1], Kohei Masunaga[a], Yasuhiko Sakai[a], Keiko Irie[b], Koji Iwano[a] and Koji Nagata[c]

[a] *Department of Mechanical Science and Engineering, Nagoya University*

[b] *Neurosurgery, Nagoya Kyoritsu Hospital*

[c] *Department of Aerospace Engineering, Nagoya University*

Correspondence author

Yasumasa Ito

Mailing address: Department of Mechanical Science and Engineering, Nagoya University, Furo-cho, Chikusa-ku, Nagoya, Aichi 464-8603, Japan

FAX & TEL: +81-(0)52-789-4488

E-mail address: yito@nagoya-u.jp

[1] Corresponding Author.

Preliminary results of this study were presented at the Annual Convention of Japanese Society of Biorheology (2014) and J. Jpn. Soc. Biorheol. 28(2) (2014)), but the submission is based upon the conference paper with enough changes to be considered as a new work.

Abstract. BACKGROUND: Stent placement can change the hemodynamics in basilar artery aneurysms. However, the effects of the stent placement can change depending on the angle of vessel bifurcation.

OBJECTIVE: The hemodynamics in and near the aneurysm are investigated for two angles of vessel bifurcation and two stent models. Some statistical indexes are also calculated to evaluate the effects of the stent placements on the possibility of aneurysm rupture.

METHODS: Computational fluid dynamics simulations and phantom model experiments are performed. The angle between the basilar and posterior cerebral arteries is set to 90 and 135 degrees. The single stent and Y stent models are tested in addition to the case without stent placement.

RESULTS: The velocity in the aneurysm in the Y stent case is smaller than that in the no stent and single stent cases when the angle is 135 degrees. High OSI and low AFI areas often appear at the same locations, and the area is larger in the single stent case than in the no stent and Y stent cases.

CONCLUSIONS: The Y stent placement promotes hemostasis and thrombosis in the basilar artery aneurysm, whereas the single stent placement can enhance growth and cause aneurysm rupture.

Keywords. Basilar artery aneurysm, Hemodynamics, Stent, Computer simulation

Introduction

Endovascular treatment has become a standard method for cerebral aneurysms due to its advantage of being less invasiveness than other treatments. The most popular endovascular treatment is coil embolization, which promotes cerebral aneurysm thrombosis. However, there is a potential risk that the coil comes off, particularly when the neck of the cerebral aneurysm is wide. Therefore, specially-designed stents for intracranial circulation, such as Enterprise VRD stent (Cordis, Miami, FL, USA), are often used to cover the neck and hold the coil in the aneurysm. In basilar artery aneurysms, in which an aneurysm is generated at the vessel bifurcation point where a basilar artery divides to two posterior cerebral arteries, single stent and Y stent models are available. Here, the single stent model has a straight shape and is placed from the basilar artery to the posterior cerebral artery, while the Y stent model has a literal Y shape and is placed from the basilar artery to the branched posterior cerebral arteries. In addition to such a function, however, it has been found that these stent models change the hemodynamics in the cerebral aneurysms. For example, Tremmel et al. [1] have shown by computational fluid dynamics (CFD) simulation that the stent placement changes the flow structure in a cerebral aneurysm and decreases flow velocity, vorticity and wall shear stress. Kono et al. [2] have investigated hemodynamics in and near a basilar artery aneurysm with the following 8 stents placement: single stent model, which is set from a proximal vessel to a right or left distal vessel; a horizontal stent model, which is placed only in the branched distal vessels; a kissing Y stent model with a uniformly narrowed structure at basilar artery; a non-overlapping Y stent model with non-crossing two stents' Y-shaped configuration; a virtual-Y stent model with no narrowed structure (fusion of 2 the single stents); and 2 different crossing-Y stent

models with a focally narrowed structure. The study shows that stent configurations significantly affect flow characteristics. Among the 8 stent models, kissing- and crossing-Y stent models reduce the inflow velocity to the aneurysm and enhance redirection of the flow to the distal vessels because of the lower stent porosity. Accordingly, wall shear stress (WSS) on the aneurysm wall decreases. Babiker et al. [3] have experimentally revealed that placement of a Y stent and cross-bar stent can significantly lower the velocity into the cerebral aneurysm in comparison to the case without the stent. Luo et al. [4] showed a strong relationship between low flow velocity into the aneurysm due to stent assistance and low recanalization rate in clinical practice. Cekirge et al. [5] showed that Y stent of the Enterprise mesh geometry without a coil significantly diverts flow, provides for a successful and stable aneurysm occlusion, and reduces the recanalization rate.

As shown above, stent placement significantly affects the hemodynamics in and near the aneurysm, which is directly related to the recanalization rate. However, in practice, the angle of vessel bifurcation varies case by case. Since the angle modifies the hemodynamics [6], the stent placement as well as the angle of vessel bifurcation should be taken into consideration to assess the effectiveness of the stent placement. In fact a numerical study on sidewall cerebral aneurysms by Kono et al. [7] indicates that the vessel curvature significantly affects hemodynamics more than stent placement. In this paper, therefore, the hemodynamics for two angles of vessel bifurcation and two stent models are investigated (in addition to the case without the stent placement) by computational fluid dynamics (CFD) simulations and phantom model experiments.

1. Materials and methods

1.1 Computational configuration

Figure 1 shows the schematic of the computational configuration. Two models of a basilar artery aneurysm are tested. In Type A, the angle between the basilar and posterior cerebral arteries is set to 90 degrees while that in Type B is set to 135 degrees. In both cases, the diameters of the basilar artery and posterior cerebral artery are 4 mm and 3 mm, respectively. The diameter of the aneurysm is 7 mm and the size of aneurysm neck is 4 mm; therefore the aspect ratio of the diameter of aneurysm neck to the height of aneurysm dome is 1.59. The lengths of basilar and posterior cerebral arteries in Type A are 18.2 mm and 28.5 mm, respectively, while those of the whole of Type B are 20.4 mm and 27.3 mm, respectively.

With regard to the stent configuration, two stent models are tested in addition to the case without the stent placement (hereinafter referred to as the no stent model). In the first model (hereinafter referred to as the single stent model), the stent is placed from the basilar artery to the left posterior cerebral artery. On the other hand, the second model (hereinafter referred to as the Y stent model) consists of two stents: The first stent is placed in the same way as the single stent model, but there is an opening in the middle of the stent. The second stent is tightly fitted inside the first stent at the basilar artery and extended to the right posterior cerebral artery through the opening. Regarding the mesh type of the stents, the Enterprise VRD stent is employed. Since we were unable to obtain the mesh pattern numerical data (except for the wire diameter), it was reconstructed from the data obtained by Micro-CT scanning. The mesh design is based on two spline curves and trigonometric function, and the blockage ratio is 7.0%.

The diameter of the stent strut is 0.05 mm and each mesh size is about 1.7 mm x 1.2 mm.

The computational domain is constructed based on a tetra mesh system. The total number of grids is about 3.5 million. The standard mesh size is 0.2 mm, but refined meshes (0.03mm at the finest points) are applied around the stent.

With regards to the coordinate system, *x* denotes the horizontal direction parallel to the posterior cerebral arteries in Type A, *y* denotes the vertical direction, and *z* denotes the direction which is perpendicular to the model.

1.2 Numerical details

Large eddy simulation (LES) is performed to solve the flow using OpenFOAM. The governing equations are filtered equation of continuity and Navier–Stokes equation;

$$\frac{\partial \bar{u}_i}{\partial x_i} = 0, \tag{1}$$

$$\frac{\partial \bar{u}_i}{\partial t} + \frac{\partial (\bar{u}_i \bar{u}_j)}{\partial x_j} = -\frac{1}{\rho}\frac{\partial \bar{p}}{\partial x_i} + \frac{\partial}{\partial x_j}\left[-\tau_{ij} + \nu\left(\frac{\partial \bar{u}_i}{\partial x_j} + \frac{\partial \bar{u}_j}{\partial x_i}\right)\right], \tag{2}$$

where p is the pressure, ρ is the density of fluid, ν is the kinematic viscosity, $\bar{u}_i$ is the velocity component larger than the grid scale, τ_{ij} is the sub-grid scale tensor. Here *i*, *j* and *k* represent *x*, *y*, and *z* directions, respectively, in Fig. 1. For sub-grid scale (SGS) modeling, the wall adapting local eddy viscosity (WALE) model [8] is applied. In the WALE model,

$$\tau_{ij} = -2\nu_t \bar{S}_{ij}, \tag{3}$$

$$\bar{S}_{ij} = \frac{1}{2}\left(\frac{\partial \bar{u}_i}{\partial x_j} + \frac{\partial \bar{u}_j}{\partial x_i}\right), \tag{4}$$

$$\nu_t = (C_w\Delta)^2 \frac{\left(S_{ij}^d S_{ij}^d\right)^{\frac{3}{2}}}{\left(\bar{S}_{ij}\bar{S}_{ij}\right)^{\frac{5}{2}} + \left(S_{ij}^d S_{ij}^d\right)^{\frac{5}{4}}}, \quad (5)$$

$$S_{ij}^d = \frac{1}{2}\left[\left(\frac{\partial \bar{u}_i}{\partial x_j}\right)^2 + \left(\frac{\partial \bar{u}_j}{\partial x_i}\right)^2\right], \quad (6)$$

where C_w is a model parameter related to Smagorinsky constant and has the value of 0.544, and Δ is sub-grid characteristic length scale. The fluid simulated in the present study is Newtonian fluid with a density of 1050 kg/m^3 and a viscosity of 3.47 × 10^{-3}Pa·s. The fluid flows into the basilar artery from the bottom with a uniform velocity in cross section and flows out from the posterior cerebral arteries. Neumann boundary conditions are applied for pressure at the inlet and for velocity at the outlets. At the outlets, pressure is set to 80 mmHg. The no-slip condition is applied to the vessel surfaces. The time variation of the inflow rate is shown in Fig. 2. The waveform of the flow is the same as the one used in Kojima et al [9,10]. Reynolds number defined by

$$Re = \frac{DU}{\nu} \quad (7)$$

is 223-571. Here D is diameter of artery inlet, U is flow rate, and ν is kinematic viscosity [9]. The time advancement of the computation is set to 0.001s.

1.3 PIV experiments

Experiments are also carried out to verify the numerical simulations. Figures 3 (A) and (B) are the photo images of the silicone phantom models of basilar artery aneurysms. The models are rigid. We also tested both Types A and B, but the model size was scaled up to 3 times larger than that of the computational domain (the typical human body size) to increase the measurement accuracy. In other words, the basilar artery diameter and posterior cerebral artery diameter are 12 mm and 9 mm, respectively. Also the aneurysm diameter is 21 mm, while the size of aneurysm neck is 12 mm.

The Enterprise VRD stent model is made by rolling up a stainless steel mesh sheet. It is also scaled up according to the model scale-up. Figure 4 (A) shows the mesh design of the sheet. The length and width of the sheet are 90 mm and 37.7 mm, respectively, and each mesh size is 5.2 mm x 3.6 mm. Figure 4 (B) shows the Y stent model. As explained earlier, the stent extends into one branch and the second stent is deployed through the hole, which follows symmetrical fracturing of struts to form a Y configuration.

Figure 5 shows a schematic of the experimental apparatus. The flow system consists of a tank, pumps, the silicon phantom model, and a flow meter. The fluid is introduced to the phantom model through 12 mm diameter tubing. The working fluid used in the present experiment is an aqueous solution made with glycerol and water at a 3:2 mixing ratio. Note that polystyrene particles coated by Rhodamine B are mixed as tracers in the fluid for particle image velocimetry (PIV). The specific gravity and diameter of the tracers are 1.1 and 15 μm, respectively. By setting the fluid temperature to a constant value of 40 deg C, the fluid density and viscosity are kept a constant value of 1050 kg/m^3 and 3.47 × 10^{-3}Pa·s, respectively. Thus the refraction index of the fluid becomes the same as that of the silicon model. This minimizes laser scatter at the model surface. The pulsating flow is formed by using a combination of a static pump and pulsatile pump. The pulsatile pump is controlled by an electric slide actuator (Oriental Motor EZHC-05A) based on an operating program (VEXTA MEXP01). The flow rate is monitored by a flow meter (Keyence FD-SS2A). The images are captured at 500 fps by a high-speed video camera (Ditect HAS-500). Note that a long-wave pass filter (>550 nm) is attached at the camera lens to capture only the fluorescence from the tracer particles. A continuous Nd: YAG laser (wavelength: 532 nm; Dantec Dynamics

RayPower 2000) sheet is used as the light source. It is introduced from the top of the phantom model to illuminate the *xy*-plane at the center of the aneurysm (z=0).

As for the inlet flow condition, to ensure the similarity of the flow characteristics in the scaled-up models, the Reynolds number and Womersley number are set to match the simulation (or real human) ones [9,10]. Womersley number is defined by

$$Wo = D\sqrt{\frac{\omega}{\nu}}, \tag{8}$$

where ω is a frequency and Wo=2.667 according to the inflow data in Fig. 2. As in Fig. 6, the time cycle is set to 6.99s.

2. Results

2.1 Verification of the CFD simulations

Figure 7 shows the mean velocity distribution in the cerebral aneurysm for the Y stent case obtained by the (A) CFD simulations and (B) experiments. Though the values are different between the experimental and numerical results due to the difference of scales, the flow patterns generally agree well, indicating that the present CFD simulations are reliable. The minor differences of the flow pattern in the aneurysm may be caused by the relatively thick laser sheet (1mm) with respect to the aneurysm (8mm).

2.2 Numerical results

Figure 8 shows the instantaneous velocity vector and contour map of the flow at t = 0.3 s, when the inlet flow rate is the largest. The inflow velocity of Type B is smaller than that of the no stent case, Type A. This result is consistent with the past study [11]. In the single and Y stent models, on the other hand, it is clear that the stents modify flow patterns drastically. Comparing the two cases with the stent placement in Type A, it

can be said that the Y stent model works better than the single stent model for the following reasons: (1) the velocity in the deep region of the aneurysm is smaller and (2) the inflow velocity at the neck is smaller in the Y stent model case, as seen in the clinical study [6]. The single stent model also reduces the velocity in comparison with the no stent case, but a high velocity region remains around the center of the neck. In Type B, the Y stent model is more effective as well as in Type A since the velocity in the aneurysm is generally smaller than that in the other two cases. This agrees with past studies [2,3]. On the contrary, there is a jet-like flow which almost reaches the center of the aneurysm in the single stent case. Considering that this flow can push the coil, which is supposed to be inserted later deeper in the aneurysm, the single stent model can make the situation worse when the angle is large; however there are also primary positive effects in that it relieves arterial constriction and prevents coil drop [12-14].

Figure 9 shows the distribution of the absolute value of instantaneous wall shear stress (WSS) at t=0.3s.

$$\mathrm{WSS} = |\mathrm{WSS}_i|, \tag{9}$$

$$\mathrm{WSS}_i = \mu \frac{\partial \bar{v}}{\partial x_n}\Big|_{\mathrm{wall}}, \tag{10}$$

where WSS_i is the instantaneous wall shear stress vector, μ is the viscosity, $\bar{v}$ is the instantaneous velocity vector larger than the grid scale, and n is the direction normal to the wall. In the no stent case, the WSS in Type A is higher than that of Type B. In Type A, the WSS decreases by the stent placement, especially in the single stent case. On the other hand, in Type B, the change in WSS by the stent placement is not as drastic as that in Type A. The WSS in the Y stent case in Type B is the largest among all cases with stent placement. We cannot conclude which case is the most critical or if the stent placement works positively or negatively here since the wall shear stress as an index

for aneurysm rupture is still an open-ended question, i.e., some studies concluded that high wall shear stress tends to enlarge the aneurysm [15-17] whereas some concluded that low wall shear stress can cause aneurysm explosion [16,18,19].

In addition to WSS, we calculated aneurysm-formation indicator (AFI) and oscillatory shear index (OSI) as risk indexes of aneurysms. The AFI is an index that evaluates the directional variation of WSS fluctuation in time and expressed by the following equation,

$$\mathrm{AFI} = \frac{\mathrm{WSS}_i \cdot \mathrm{WSS}_{av}}{|\mathrm{WSS}_i||\mathrm{WSS}_{av}|}, \tag{11}$$

where WSS_{av} is the time-averaged WSS vector. It is reported that a bleb is preferentially generated at low AFI area [20]. In addition, OSI is defined by

$$\mathrm{OSI} = \frac{1}{2}\left\{1 - \frac{\left|\int_0^T \mathrm{WSS}_i dt\right|}{\int_0^T |\mathrm{WSS}_i| dt}\right\}, \tag{12}$$

where T is the time cycle of the pulsatile flow. A high OSI indicates vascular inflammation through macrophage activation, in addition to apoptosis due to vascular endothelial disarray [21,22].

Figure 10 shows the distribution of AFI at t=0.3s. Regardless of the angle of vessel bifurcation, the single stent cases have a larger area of low AFI compared to other cases. Though the AFI distribution is different between the no stent and Y stent cases, the difference is not significant from a bleb formation point of view.

Figure 11 shows the distribution of OSI. Regardless of the angle of vessel bifurcation, larger high-OSI areas appear at multiple locations in the single stent case, while such regions do not appear in the no stent and Y stent cases.

It must also be emphasized that comparison of Figs. 10 and 11 reveal that high OSI and low AFI areas often appear at the same locations in the single stent case. This

means that a bleb can generate at where the vessel is damaged, which is quite dangerous.

3. Discussion

The present study shows that the Y stent model works positively by reducing the inflow velocity to the aneurysm (Fig. 8) whereas the single stent model can work negatively in some cases (Figs. 8, 10, and 11). In addition, by comparing Types A and B with in terms of Y stent placement, we find that the flow velocity distribution in Type B (in which the angle is 135 degrees) is better than that in Type A (90 degrees) because the flow velocity in the posterior cerebral arteries in Type B is larger than in Type A. Past clinical study [5] shows that the Y stent placement decreases the angle between left- and right-posterior cerebral arteries (i.e. increases the angle between the basilar and posterior arteries). Thus our study indicates that the Y stent placement has two advantages: (1) increasing the angle between the basilar and posterior arteries, thus decreasing the inflow velocity to the aneurysm, which results in (2) enhancing blood flow directly into the posterior cerebral arteries and reducing the inflow velocity to the aneurysm. Both changes contribute to hemostasis and aneurysm thrombosis. In addition, considering that the risk of stenosis due to Y stent placement is minimal [5,23,24], it should be encouraged to employ Y stents rather than single stents for basilar artery aneurysm.

4. Conclusion

In this paper, the hemodynamics in and near a basilar artery aneurysm is investigated by CFD simulations and experiments. The angle between the basilar and posterior cerebral arteries is set to 90 or 135 degrees. With regard to the stent configuration, the

single stent and Y stent models are tested in addition to one with no stent. The results show that the inflow velocity to the aneurysm in the 135 degree case is smaller than that in the 90 degree case in the no stent and Y stent cases. The velocity in the aneurysm in the Y stent case is generally smaller than those in both the no stent and single stent cases when the angle is 135 degrees. Larger high-OSI and low-AFI areas appear in the single stent case, often at the same locations, in comparison to the no stent and Y stent cases. These observations suggest that the Y stent placement promotes the hemostasis and aneurysm thrombosis. On the other hand, the single stent placement can enhance growth and rupture of basilar artery aneurysm particularly when the angle of vessel bifurcation is large; however there are positive effects in that it relieves arterial constriction and prevents coil drop. The present results can be applied only to limited conditions but indicates the possibility in practical use. The present results can be applied only to limited conditions but indicates the possibility in practical use.

Acknowledgements

We appreciate Mr. Raymond Roman (UCLA) for his help in preparing the paper.

References

[1] Tremmel M, Xiang J, Natarajan SK, Hopkins LN, Siddiqui AH, Levy EI, et al. Alteration of intra-aneurysmal hemodynamics for flow diversion using enterprise and vision stents. World neurosurgery. 2010; 74: 306-315.

[2] Kono K, Terada T. Hemodynamics of 8 different configurations of stenting for bifurcation aneurysms. Am J Neuroradiol. 2013; 34: 1980-1986.

[3] Babiker MH, Gonzalez LF, Ryan J, Albuquerque F, Collins D, Elvikis A, et al. Influence of stent configuration on cerebral aneurysm fluid dynamics. J Biomech. 2012; 45: 440-447.

[4] Luo B, Yang X, Wang S, Li H, Chen J, Yu H, et al. High shear stress and flow velocity in partially occluded aneurysms prone to recanalization. Stroke. 2011; 42(3): 745-753.

[5] Cekirge HS, Yavuz K, Geyik S, Saatci I. A novel "Y" stent Flow Diversion Technique for the Endovascular Treatment of Bifurcation Aneurysms without Endovascular Coiling. Am J Neuroradiology. 2011; 32: 1262- 1268.

[6] Gao B, Baharoglu MI, Cohen AD, Malek AM. Y stent Coiling of Basilar Bifurcation Aneurysms Induces a Dynamic Angular Vascular Remodeling With Alteration of the Apical Wall Shear Stress Pattern. Neurosurgery. 2013; 72: 617-629.

[7] Kono K, Shintani A, Terada T. Hemodynamic Effects of Stent Struts versus Straightening of Vessels in Stent-Assisted Coil Embolization for Sidewall Cerebral Aneurysms. PLoS One. 2014; 9: e108033.

[8] Nicoud F, Ducros F. Subgrid-scale stress modelling based on the square of the velocity gradient tensor. Flow, Turbulence and Combustion. 1999; 62(3): 183-200.

[9] Kojima M, Irie K, Ikeda S, Fukuda T, Arai F, Hirose Y, et al. The hemodynamic study for growth factor evaluation of rupture cerebral aneurysm followed up for five years. Journal of Biomedical Science and Engineering. 2012; 5(12): 884.

[10] Kojima M, Irie K, Masunaga K, Sakai Y, Nakajima M, Takeuchi M, et al. Hybrid stent device of flow-diverting effect and stent-assisted coil embolization formed by

fractal structure. Medical & Biological Engineering & Computing. 2016; 54(5): 831-841.

[11] Roach MR, Scott S, Ferguson GG. The hemodynamic importance of the geometry of bifurcations in the circle of Willis (glass model studies). Stroke. 1972; 3(3): 255-267.

[12] Ansari SA, Lassig JP, Nicol E, Thompson BG, Gemmete JJ, Gandhi D. Thrombosis of a fusiform intracranial aneurysm induced by overlapping Neuroform stents: case report. Neurosurgery. 2007; 60: E950-951

[13] Mehta B, Burke T, Kole M, Bydon A, Seyfried D, Malik G. Stent-within-a-stent technique for the treatment of dissecting vertebral artery aneurysms. AJNR Am J Neuroradiol. 2003; 24:1814-1818

[14] Brassel F, Rademaker JHaupt C, Becker H. Intravascular stent placement for a fusiform aneurysm of the posterior cerebral artery: case report. Eur Radiol. 2001: 1250-1253

[15] Tateshima S, Murayama Y, Villablanca JP, Morino T, Nomura K, Tanishita K, Vinuela F. In vitro measurement of fluid-induced wall shear stress in unruptured cerebral aneurysms harboring blebs. Stroke. 2003; 34(1): 187-192.

[16] Tateshima S, Tanishita K, Omura H, Villablanca JP, Vinuela F. Intra-aneurysmal hemodynamics during the growth of an unruptured aneurysm: in vitro study using longitudinal CT angiogram database. Am J Neuroradiology. 2007; 28(4): 622-627.

[17] Shojima M, Oshima M, Takagi K, Torii R, Hayakawa M, Katada K, Morita A, Kirino T. Magnitude and role of wall shear stress on cerebral aneurysm computational fluid dynamic study of 20 middle cerebral artery aneurysms. Stroke. 2004; 35(11): 2500-2505.

[18] Meng H, Wang Z, Hoi Y, Gao L, Metaxa E, Swartz DD, Kolega J. Complex hemodynamics at the apex of an arterial bifurcation induces vascular remodeling resembling cerebral aneurysm initiation. Stroke. 2007; 38(6): 1924-1931.

[19] Malek AM, Alper SL, Izumo S. Hemodynamic shear stress and its role in atherosclerosis. Jama. 1999; 282(21): 2035-2042.

[20] Mantha A, Karmonik C, Benndorf G, Strother C, Metcalfe R. Hemodynamics in a cerebral artery before and after the formation of an aneurysm. Am J Neuroradiology. 2006; 27: 1113-1118.

[21] Omodaka S, Sugiyama S, Inoue T, Funamoto K, Fujimura M, Shimazu H, et al. Local hemodynamics at the rupture point of cerebral aneurysms determined by computational fluid dynamic analysis. Cerebrovascular Diseases. 2012; 34: 121-129.

[22] Ku DN, Giddens DP, Zarins CK, Glagov S. Pulsatile flow and atherosclerosis in the human carotid bifurcation. Positive correlation between plaque location and low oscillating shear stress. Arteriosclerosis, thrombosis, and vascular biology. 1985; 5(3): 293-302.

[23] Makoyeva A, Darsaut T, Salazkin I, Raymond J. Y-Crossing of Braided Stents with Stents and Flow Diverters Does not Cause Significant Stenosis in Bench-Top Studies. Interventional Neuroradiology. 2013; 19: 455-460.

[24] Alejandro S, Jonathan L, Imran C, Raymond T, Aquilla T. Y-Stenting for Bifurcation Aneurysm Coil Embolization:What is the Risk?. Stroke Research and Treatment. 2014; 762389.

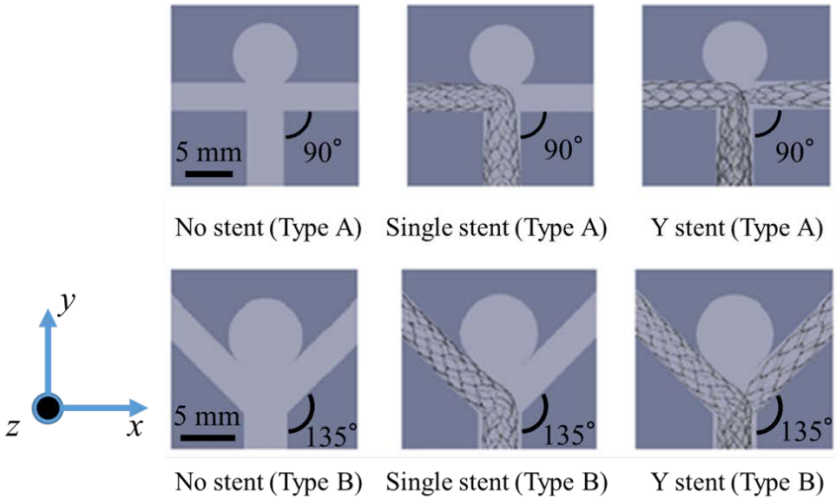

Fig. 1 Basilar artery aneurysm models and stent models for CFD simulations. The angle between basilar artery and posterior cerebral arteries is 90 and 135 degrees in Types A and B, respectively.

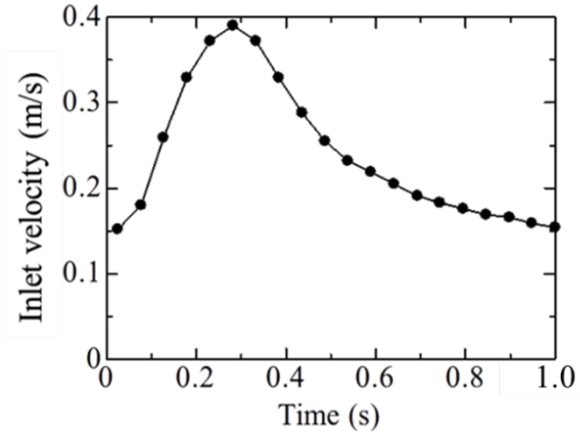

Fig. 2 Waveform of the inlet velocity for the CFD analysis.

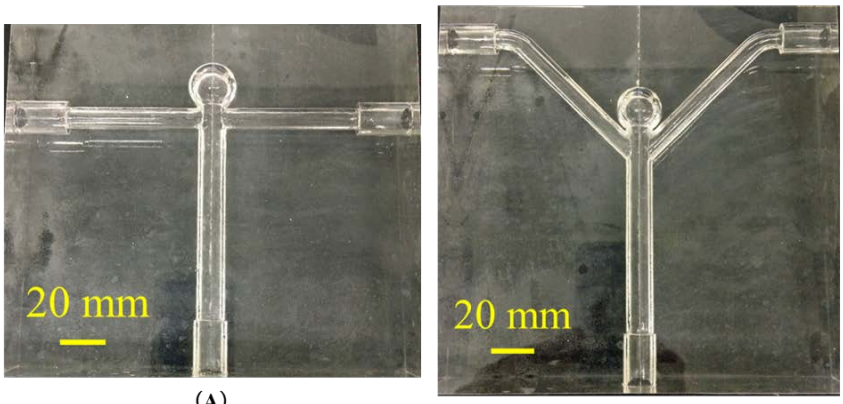

Fig. 3 Basilar artery aneurysm models for experiments. (A) Type A, (B) Type B.

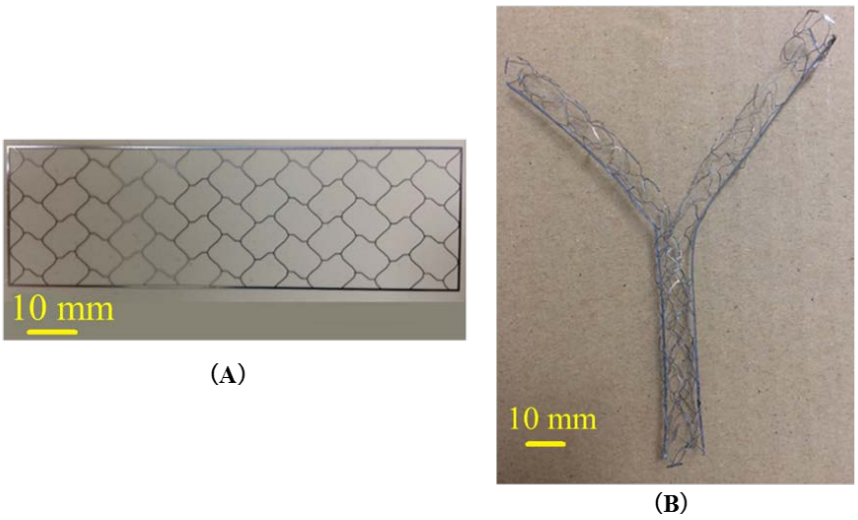

Fig. 4 Stent sheet and model. (A) Stent sheet of Enterprise VRD, (B) the Y stent model.

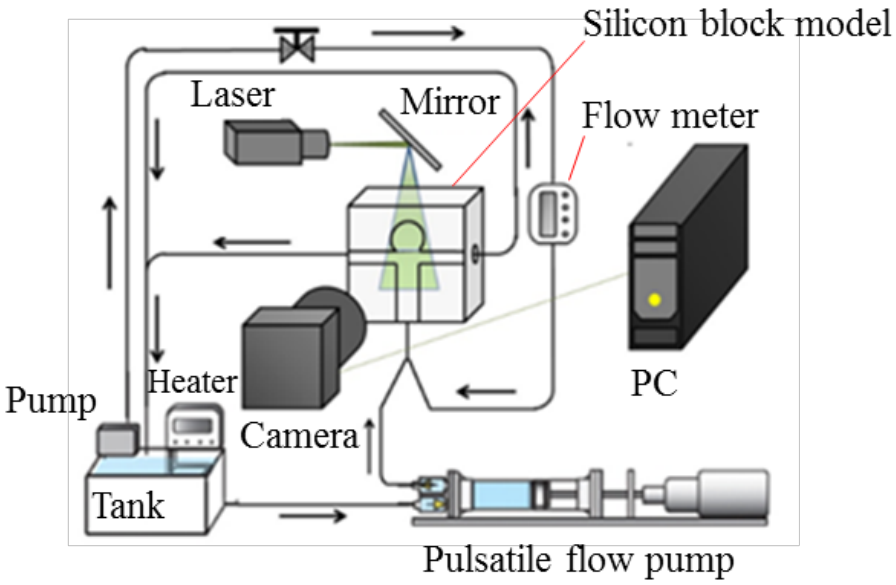

Fig. 5 Schematic of the experimental apparatus.

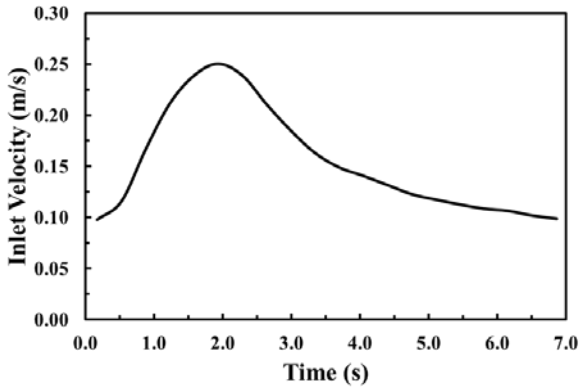

Fig. 6 Waveform of the inlet velocity for experiments.

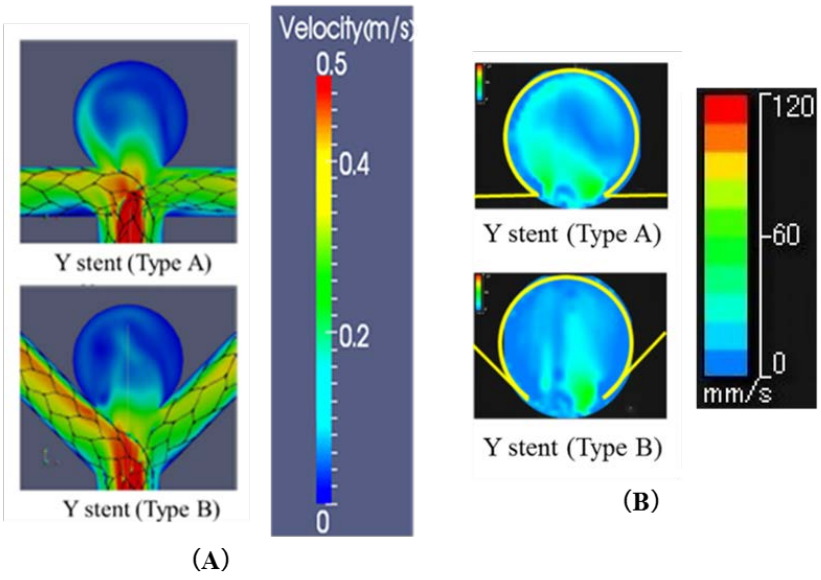

Fig. 7 Mean flow velocity on the *xy*-plane at the center of the cerebral aneurysm. (A) CFD results; (B) experimental results.

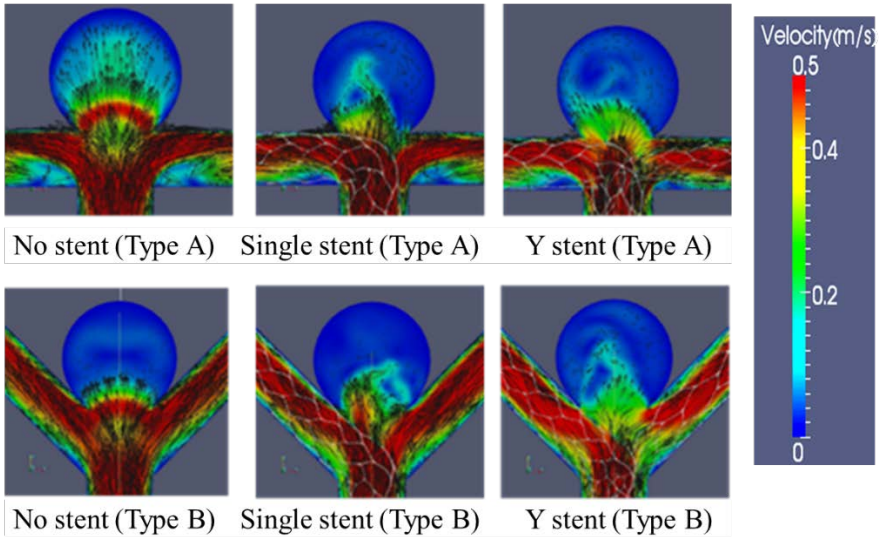

Fig. 8 Velocity vector and contour map at *t*= 0.3s.

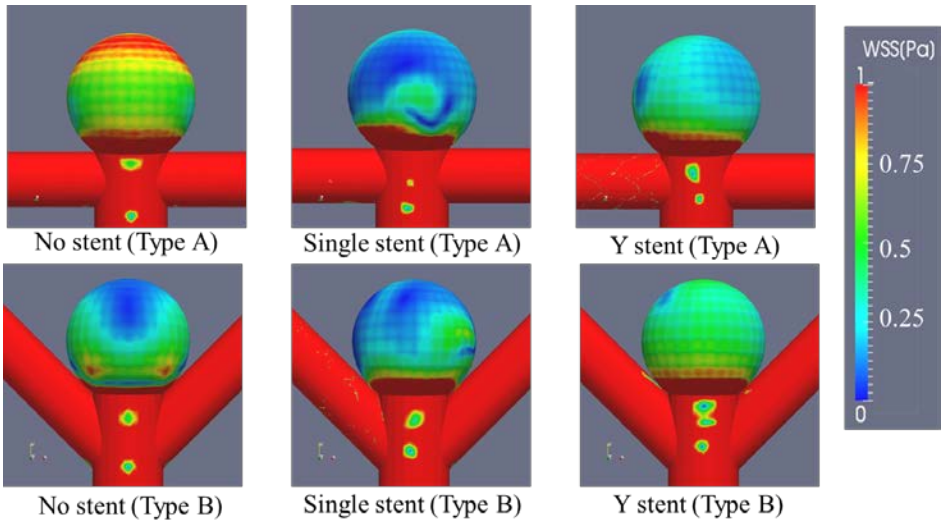

Fig. 9 Distribution of WSS at *t* = 0.3s.

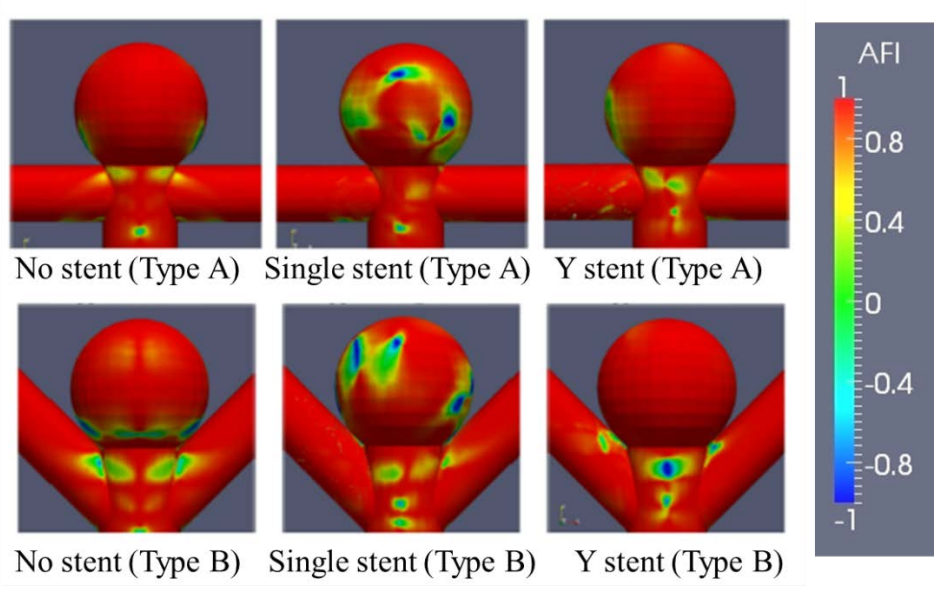

Fig. 10 Distribution of AFI at t = 0.3s.

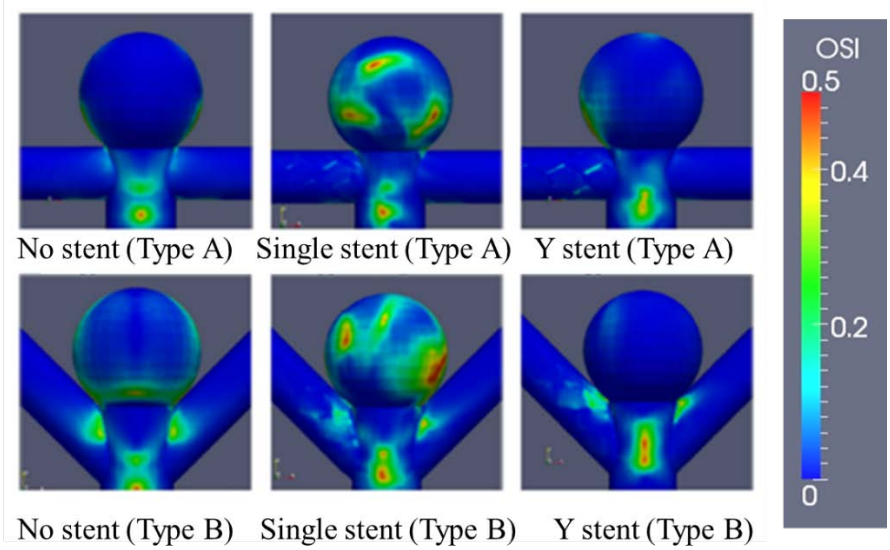

Fig. 11 Distribution of OSI.